

## Wave chaos in elastodynamic cavity scattering

A. WIRZBA<sup>1</sup>, N. SØNDERGAARD<sup>2</sup> and P. CVITANOVIĆ<sup>3</sup>

<sup>1</sup> *Institut für Kernphysik, Forschungszentrum Jülich - D-52425 Jülich, Germany*

<sup>2</sup> *Matematisk Fysik, Lunds Universitet - Box 118, SE-22100 Lund, Sweden*

<sup>3</sup> *Center for Nonlinear Science, School of Physics, Georgia Institute of Technology Atlanta, GA 30332-0430, USA*

received 29 June 2005; accepted in final form 26 September 2005

published online 14 October 2005

PACS. 05.45.Mt – Quantum chaos; semiclassical methods.

PACS. 46.40.Cd – Mechanical wave propagation (including diffraction, scattering, and dispersion).

PACS. 62.30.+d – Mechanical and elastic waves; vibrations.

**Abstract.** – The exact elastodynamic scattering theory is constructed to describe the spectral properties of two- and more- cylindrical cavity systems, and compared to an elastodynamic generalization of the semi-classical Gutzwiller unstable periodic orbits formulas. In contrast to quantum mechanics, complex periodic orbits associated with the surface Rayleigh waves dominate the low-frequency spectrum, and already the two-cavity system displays chaotic features.

*Introduction.* – The Gutzwiller semi-classical quantization of classically chaotic systems relates quantum observables such as spectral densities to sums over classical unstable periodic orbits [1, 2]. The work presented here is a step toward a formulation of such approximate short-wavelength theory of wave chaos for the case of linear elastodynamics. Why elastodynamics? The experiments initiated in ref. [3] attain  $Q$  values as high as  $5 \cdot 10^6$ , making spectral measurements in elastodynamics competitive with measurements in microwave cavities at liquid-helium temperatures [4, 5], and vastly superior to nuclear-physics and room temperature microwave experiments for which the  $Q$  values are orders of magnitude lower, typically  $\sim 10^2$ – $10^3$ . For elastodynamics there are only a few experimental demonstrations [6] of the existence of unstable periodic orbits, and no theory that would predict them. While Oxborrow *et al.* [3] measure about  $10^5$  spectral lines, the current theory is barely adequate for computation of dozens of resonances. A more effective theory would find many applications such as in the frequency domain quality testing for small devices built from high- $Q$  materials. This unsatisfactory state of affairs is the *raison d'être* for the theoretical effort undertaken here.

While current experiments excel in measurements of eigenspectra of *compact resonators*, the periodic orbit theory computations of such bound system spectra are rendered difficult by the presence of non-hyperbolic phase space regions. As our primary goal is to derive and test rules for replacing wave mechanics by the short-wavelength ray-dynamic trajectories, we concentrate here instead on the problem of *scattering* off cylindrical cavities, for which the classical dynamics is fully under control. In the case of one cavity the exact scattering spectrum is known [7]. For the multiple-cavities case we generalize the quantum-mechanical (QM) S-matrix formalism for  $N$ -disk scattering [8–11], and compute the exact resonances and the Wigner time delays from the full elastodynamic wave-mechanical scattering matrix. We then

compare the exact results with the corresponding quantities calculated in the short-wavelength approximation (SWA), and discover that the QM intuition fails us: the Rayleigh surface waves (which have no analog in the QM scattering problem) dominate the low-frequency spectrum because of their weights and number, such that already the two-disk elastodynamic scattering problem displays chaotic features in this regime in contrast to its QM counterpart.

*Elastodynamics.* – Consider an infinite slab of an isotropic and homogeneous elastic material (*e.g.*, polyethylene or isotropic quartz) with parallel top and bottom plane boundaries, and an in-phase stimulus such that the system behaves quasi-two-dimensionally along the slab, with no excitation of or coupling to waves propagating perpendicular to the slab. The propagating waves are either the pressure or the shear solutions of the Navier-Cauchy equation [12]  $\mu \nabla^2 \mathbf{u} + (\lambda + \mu) \nabla (\nabla \cdot \mathbf{u}) + \rho \omega^2 \mathbf{u} = \mathbf{0}$ , where  $\mathbf{u}$  is a vectorial displacement field,  $\lambda$  and  $\mu$  are the Lamé constants,  $\rho$  the mass density and  $\omega$  the frequency. The experiments dictate free boundary conditions, with vanishing traction  $\mathbf{t}(\mathbf{u}) = \mathbf{0}$ , where

$$\mathbf{t}(\mathbf{u}) \equiv \left[ \lambda (\nabla \cdot \mathbf{u}) \mathbb{1} + \mu \left\{ (\nabla \mathbf{u}) + (\nabla \mathbf{u})^T \right\} \right] \cdot \hat{\mathbf{n}}. \quad (1)$$

Here  $\hat{\mathbf{n}}$  is a unit vector normal to the boundary,  $\mathbb{1}$  the unit matrix, and T indicates a transposition. Elastodynamic waves are vectorial, with the pressure (longitudinal, L) wave propagating through the bulk with velocity  $c_L = \sqrt{(\lambda + 2\mu)/\rho}$ , and the shear (transverse, T) wave with velocity  $c_T = \sqrt{\mu/\rho}$ . Furthermore, the Rayleigh surface waves propagate along plane boundaries unattenuated, with the velocity  $c_R$  determined [12] by the condition

$$0 = (2\eta^2 - 1)^2 - 4\eta^2 \sqrt{(\eta^2 - 1)(\eta^2 - (c_T/c_L)^2)} \quad \text{with} \quad \eta \equiv c_T/c_R. \quad (2)$$

When either a shear or pressure plane wave hits a boundary, mode conversion can take place [13], with waves of different types emitted at different angles. We now drill one, two, or more cylindrical cavities of radius  $a$  perpendicularly through the slab.

*One-cavity scattering, the exact spectrum.* – Scattering off a single cylindrical cavity is separable in angular momentum. The one-cavity S-matrix of elastodynamics, a  $[2 \times 2]$  matrix in  $\{L, T\}$  components, is determined by the free boundary condition for the traction matrices

$$\mathbf{S}_{mm'}^{(1)} = -\delta_{mm'} [\mathbf{t}_m^{(+)}]^{-1} \cdot [\mathbf{t}_m^{(-)}], \quad m = 0, \pm 1, \pm 2, \dots \quad (3)$$

For comparison, the corresponding one-disk scattering matrix [11, 14] of quantum mechanics (QM), for a scalar field with the Dirichlet boundary condition, is expressed in terms of Hankel functions,  $S_{mm'}^{(1)} = -\delta_{mm'} H_{m'}^{(-)}(ka)/H_m^{(+)}(ka)$ , as a function of the wave number  $k$ . The traction matrices [15] of angular momentum  $m$  and superscript  $Z \in \{+, -, J\}$  result when outgoing (+), incoming (−) or regular (J) pressure and shear displacements  $\mathbf{u}$  in terms of Hankel or Bessel functions,  $Z_m \in \{H_m^{(+)}, H_m^{(-)}, J_m\}$ , are inserted into the traction (1):

$$[\mathbf{t}_m^{(Z)}]_{\pi\sigma} = \frac{2\mu}{a^2} \left[ (-1)^\sigma \delta_{\pi\sigma} \left( k_\sigma \frac{d}{dk_\sigma} - (m^2 - \frac{1}{2} k_T^2 a^2) \right) - im(1 - \delta_{\pi\sigma}) \left( k_\sigma \frac{d}{dk_\sigma} - 1 \right) \right] Z_m(ak_\sigma). \quad (4)$$

The index  $\pi \in \{1, 2\}$  labels the 2- $d$  spherical components  $\{\hat{\mathbf{r}}, \hat{\boldsymbol{\theta}}\}$  of the displacement  $\mathbf{u}$  at the cavity while  $\sigma \in \{1, 2\}$  labels its polarization  $\{L, T\}$ , where  $k_\sigma = \omega/c_\sigma$  are the corresponding wave numbers. The scattering resonances for the one-cavity elastodynamic medium with traction-free boundary conditions are determined [7] from  $\det[\mathbf{t}_m^{(+)}] = 0$ , see eq. (3).

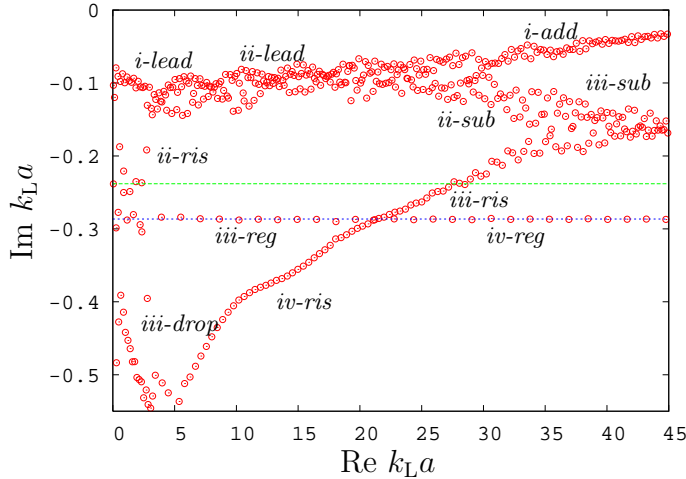


Fig. 1 – The lowest few hundred exact  $A_1$  resonances of the two-cavity elastodynamic scatterer, in the complex pressure wave number  $k_L = \omega/c_L$  plane. The labels refer to the various resonance families interpreted (together with the lines) in the *Discussion* section, where the italics specify the orders in the cumulant expansion at which the structures are first observed. The second label indicates whether the bands are *leading* (closest to the real axis), *additional*, *subleading*, *rising*, *regular* or *dropping*.

*Multi-cavity scattering, exact spectrum.* – We construct the S-matrix for the  $N$ -cavity system following ref. [11]. The determinant of the  $N$ -scatterer S-matrix factorizes, as in QM, into the product of the one-cavity determinants and the multi-scattering contributions [11,15]:

$$\det S(\omega) = \frac{\text{Det}[M(\omega^*)^\dagger]}{\text{Det}[M(\omega)]} \prod_{j=1}^N \det S^{(1)j}(\omega). \quad (5)$$

Here the matrix  $M = \mathbb{1} + A$  is the inverse of the multi-scattering matrix. The transfer matrix  $A$  evolves the displacement of internal angular momentum  $l' = 0, \pm 1, \pm 2, \dots$  and spherical component  $\pi' \in \{1, 2\}$  at cavity  $j'$  (of radius  $a_{j'}$ ) to the ( $l = 0, \pm 1, \pm 2, \dots$  and  $\pi \in \{1, 2\}$ ) displacement at cavity  $j$  (of radius  $a_j$ ) where  $j, j' = 1, \dots, N$  are the cavity labels:

$$[A_{l'l'}^{jj'}]_{\pi\pi'} = (1 - \delta_{jj'}) \frac{a_j}{a_{j'}} \sum_{\sigma=1}^2 \sum_{\sigma'=1}^2 [\mathbf{t}_l^{(j)j}]_{\pi\sigma} [\mathbf{T}_{l'l'}^{(+)(jj')}]_{\sigma\sigma'} [\mathbf{t}_{l'}^{(+)(j')}]_{\sigma'\pi'}^{-1}. \quad (6)$$

The matrix  $[\mathbf{T}_{l'l'}^{(+)(jj')}]_{\sigma\sigma'} = \delta_{\sigma\sigma'} H_{l-l'}^{(+)}(k_\sigma R_{jj'}) \exp[i l \alpha_{j'j} - i l' (\alpha_{jj'} - \pi)]$  translates the  $\{\mathbf{L}, \mathbf{T}\}$  modes evaluated relative to the origin of cavity  $j'$  to the corresponding modes at cavity  $j$ .  $R_{jj'}$  and  $\alpha_{jj'}$  are the relative center-to-center distances and angles, respectively [11,15]. The multi-scattering resonances of the  $N$ -cavity problem are given by the zeros of  $\text{Det } M(\omega)$ , see eq. (5). For the two-cavity system the two-fold reflection symmetry implies that the determinant factors into four irreducible representations, with the transfer matrix for each irreducible subspace defined on the fundamental domain, a quarter of the full elastodynamic slab [2].

Here we present typical numerical results for the fully symmetric  $A_1$  subspace of the system of two cylindrical cavities. In all presented calculations we take values of the Lamé constants corresponding to polyethylene [7], and set  $c_L = 1950$  m/s,  $c_T = 540$  m/s,  $c_R \approx 513$  m/s, and take cavities of radius  $a = 1$  cm, center-to-center separation  $R = 6$  cm. The lowest few hundred exact  $A_1$  resonances (hopefully, *all*  $A_1$  resonances in the window  $[0 < \text{Re } k_L a < 45, -0.55 < \text{Im } k_L a < 0]$ ) determined by the zeros of  $\text{Det}(\mathbb{1} + A)|_{A_1}$  are shown in fig. 1.

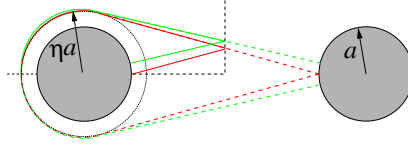


Fig. 2 – Two new periodic orbits of Rayleigh type of topological length 2 (and “effective” arc radius  $\eta a > a$ ) in the fundamental domain (and the full space) of the two-cavity system. In the former the Rayleigh orbits are further classifiable by the number of contacts with the two symmetry axes [17,18].

*One-cavity scattering, ray-dynamic interpretation.* – In the one-cavity case a sophisticated theory of ray dynamics already exists. The main tool is the Sommerfeld-Watson transformation which in the QM case replaces a slowly converging partial wave sum by a fast converging sum over *complex creeping* trajectories, first derived by Franz [14]. The pressure and shear Franz resonances also exist in elastodynamics [16], but here the one-cavity spectrum is dominated by the weakly damped Rayleigh resonances [7], with no QM counterpart.

In the spirit of Keller’s geometrical theory of diffraction [16] we use the one-cavity S-matrix (3) to assign a ray-dynamic weight to a segment of the boundary traversed by a Rayleigh wave. A circular Rayleigh segment of arc length  $\Delta\phi a$  (with  $\Delta\phi$  the pertinent angle) has the complex-valued weight  $\exp[i\Delta\phi \nu_R(\omega)]$ , such that the effective arc length of a Rayleigh segment is  $\Delta\phi \nu_R(\omega)/k_T \approx \Delta\phi a\eta$ , where  $\eta = c_T/c_R$ , see eq. (2). Here we take  $\Delta\phi$  times the *exact wave-mechanical*  $\nu_R(\omega)$ , determined as complex angular momentum by  $\det[\mathbf{t}_{\nu_R(\omega)}^{(+)}] = 0$ , as the *input* for the complex-valued action of the Rayleigh trajectory segment.

*Multi-cavity scattering, ray-dynamic interpretation.* – In QM the Gutzwiller-Voros Zeta function is the semi-classical approximation to  $\text{Det } \mathbf{M}$ , where the connection follows via the semi-classical reduction of the traces  $\text{Tr}(\mathbf{A}^n)$  appearing in the cumulant expansion  $\text{Det } \mathbf{M} = 1 + \text{Tr } \mathbf{A} - [\text{Tr } \mathbf{A}^2 - (\text{Tr } \mathbf{A})^2]/2 + \dots$ . As shown in refs. [10,11], in the SWA (applicable here from  $k_L a \sim 2$  onwards) the traces  $\text{Tr } \mathbf{A}^n$  reduce to the set of ray-dynamic periodic orbits of topological length  $n$ , whereas the cumulants become “curvatures” (periodic orbits shadowed by pseudo orbits [2]). The shortest geometrical periodic orbits, bouncing between the two cavities, are the border orbits of topological length one in the fundamental domain. Their weights, derived from the SWA to  $\text{Tr } \mathbf{A}_{A_1}$ , are of form [11, 15]  $t_\sigma = -\exp[ik_\sigma(R - 2a)]/[\sqrt{|\Lambda_0|}(-\Lambda_0)^{\sigma-1}(1 - \Lambda_0^{-2})]$  with  $\Lambda_0 = (R - a + \sqrt{R^2 - 2Ra})/a$ ,  $\sigma \in \{1, 2\} \equiv \{\text{L}, \text{T}\}$ . These unstable geometrical orbits including their repetitions are summed up in the usual way in terms of the Gutzwiller-Voros spectral determinant  $\text{Det } \mathbf{M}_{\text{geom.}}$  [2].

Moreover, Keller’s theory yields orbits with unstable geometrical legs *and* weakly damped Rayleigh surface wave arcs circling the cavities. At the topological length one, two (unstable) complex Rayleigh-type periodic orbits, an “oval” and “figure eight” contribute [10]. In addition to the repeated primary orbits *and* the “oval-eight” combination, two new (unstable) Rayleigh-type orbits contribute to  $\text{Tr } \mathbf{A}^2$ , see fig. 2 and so on for longer Rayleigh-type orbits, with their total number (including repeats) growing exponentially with their topological length. By analogy to creeping orbits [17,18], if  $q_i$ ,  $i = 1, \dots, n$  (with  $q_{n+i} \equiv q_i$ ) are the points along a cycle where a Rayleigh arc segment connects to geometric trajectories (which may include reflections with/without conversions between pressure and shear rays), the Rayleigh surface wave contribution to the spectral determinant is of form

$$\text{Det } \mathbf{M}|_{\text{Rayl.}} = \exp \left[ \sum_{p,r=1}^{\infty} (-1/r) \left( \prod_{i=1}^{n_p} [G(q_{i+1}, q_i)]_{\sigma_{i+1}\sigma_i} \right)^r \right]. \quad (7)$$

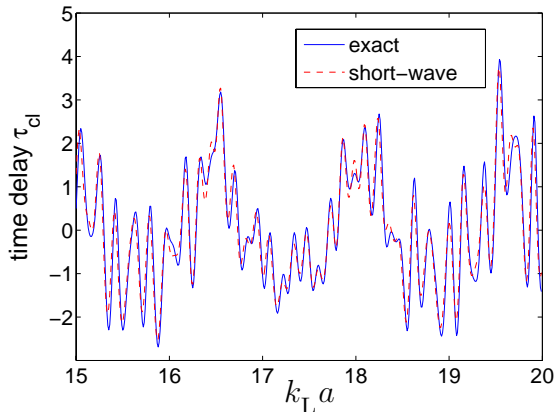


Fig. 3 – Wigner time delay for the two-cavity system, the exact  $A_1$  result *vs.* its ray-dynamic expansion to period two, as a function of the pressure wave number  $k_L$  (times the cavity radius  $a$ ).

Here the summation goes over all prime periodic orbits  $p$  and their repetition number  $r$ .  $[G(q_{i+1}, q_i)]_{\sigma_{i+1}\sigma_i}$  (with  $\sigma_i, \sigma_{i+1} \in \{L, T\}$ ) is the Van-Vleck propagator (including instabilities, reflections and mode conversions [15, 19]) if  $q_i$  and  $q_{i+1}$  are connected by a pure geometric trajectory, and  $\frac{i}{2}[\tilde{D}_R(\omega)]_{\sigma_{i+1}\sigma_i} \exp[i\Delta\phi \nu_R(\omega)]$  if  $q_i$  and  $q_{i+1}$  are the endpoints of a Rayleigh arc segment, with  $\sigma_i, \sigma_{i+1}$  the polarizations of the two attached geometrical legs. The  $[2 \times 2]$  diffraction matrix  $\tilde{D}_R(\omega)$  is the elastodynamics analogue of the *square* of the corresponding QM diffraction constant [11, 17, 18]. It is determined by Keller and Karal [16] for the half-plane case, and in [15] for the circular cavity.  $[\tilde{D}_R(\omega)]_{\sigma_{i+1}\sigma_i}$  is proportional to  $\exp[-\lambda(\omega)_{\sigma_{i+1}} - \lambda(\omega)_{\sigma_i}]$  with  $\lambda(\omega)_\sigma \equiv \nu_R \operatorname{arccosh}[\nu_R/(ak_\sigma)] - \sqrt{\nu_R^2 - (ak_\sigma)^2}$ , *i.e.*, it is weakly attenuated for the pure shear case  $\sigma_{i+1} = \sigma_i = T$  at low frequencies, but strongly attenuated otherwise.

The “semiclassical” form of the spectral determinant is given by the formal product  $\operatorname{Det} M|_{\text{geom.}} \times \operatorname{Det} M|_{\text{Rayl.}}$ , evaluated in the cycle expansion where the classifying topological length is equal to the number of geometrical straight legs of the orbits and pseudo orbits [2].

The Wigner time delays and cumulant traces are particularly well suited to detailed comparisons of the exact results with the SWA [11]. In fig. 3 we plot the exact Wigner “time” delay  $\tau_{\text{cl}} = \frac{d}{dk_L a} \eta_{\text{cl}}$  of the cluster phase shift  $\eta_{\text{cl}}(\omega) = -i \frac{1}{2} \ln [\operatorname{Det} M(\omega^*)^\dagger / \operatorname{Det} M(\omega)]$  as a function of the pressure wave number  $k_L = \omega/c_L$ , and compare it to the cycle expansion based on the geometrical and complex periodic orbits of topological lengths one and two. The periodic orbit approximation is in good agreement with the exact result which can be truncated at second cumulant order for the presented  $k_L$  values. Finally, in fig. 4 we compare the periods of the ray-dynamic periodic orbits with the Fourier peaks of the exact wave-mechanical data by plotting the moduli of the Fourier transforms of  $\operatorname{Tr} A_{A_1}$  and  $\operatorname{Tr} A_{A_1}^2$  for the region  $10 \leq k_L a \leq 45$ , and the corresponding Fourier transforms of sums over periodic orbits of topological length one and two, respectively. The Fourier peaks indeed correspond to the periodic-orbit periods  $T_p = \sum_{i_L} l_{i_L}/c_L + \sum_{i_T} l_{i_T}/c_T + \sum_{i_R} \eta a \Delta \phi_{i_R}/c_T$ , with  $l_{i_L}$ ,  $l_{i_T}$  and  $\eta a \Delta \phi_{i_R}$  the (effective) geometrical lengths of the pressure, shear and Rayleigh segments, respectively.

The SWA captures nearly all qualitative features of the exact calculation. However, the  $1/k_L a$  corrections are still not negligible, as can be seen from the small structure close to 0.1 ms in fig. 4 (right). This corresponds to a combined LT geometric orbit that vanishes in the SWA, as there is no coupling of pressure to shear rays at perpendicular impact. The complex orbits visible in fig. 4 have only shear segments coupled to Rayleigh segments, whereas the coupling of pressure segments to Rayleigh segments is severely suppressed (since  $c_L \gg c_R$ ).

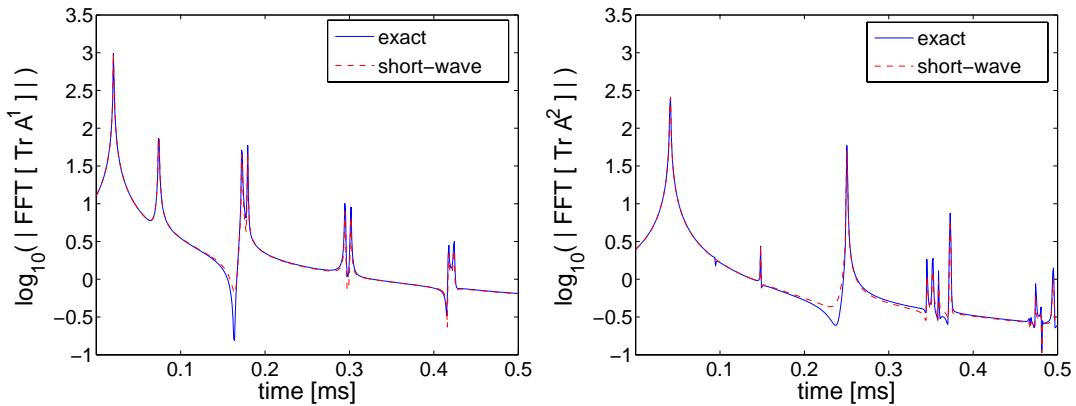


Fig. 4 – Comparison of the Fourier transforms of the exact traces  $\text{Tr } A_{A_1}$  (left panel) and  $\text{Tr } A_{A_1}^2$  (right panel) of the two-cavity system with the short-wavelength approximation (SWA) based on periodic orbits of topological length one and periodic orbits of topological length two, respectively, in the range  $10 \leq k_L a \leq 45$ . All peaks are identifiable as the periods of the shortest period orbits.

*Discussion.* – These observations combined with the cumulant expansion (in detail beyond the scope of this letter) explain the qualitative features of the low-frequency resonance spectrum shown in fig. 1. The dotted and dashed lines represent the imaginary parts  $\text{Im } k_L = -\frac{1}{2} \ln(\Lambda_0)/(R - 2a) \approx -0.29/a$  and  $\text{Im } k_T = -\frac{3}{2} \ln(\Lambda_0)c_T/c_L(R - 2a) \approx -0.24/a$  predicted by the isolated pressure  $t_L$  and shear  $t_T$  orbit, respectively. As the transverse oscillation of the  $t_T$  orbit strongly mixes with the Rayleigh waves of nearly the same wave velocity, the irregular band with the *leading* and *subleading* resonances arises from the interference of the Rayleigh orbits with the  $t_T$  orbit. Due to this mixing, there are no resonances on the  $t_T$  line.

The Rayleigh orbits include the factor  $(1 - \exp[2\pi i \nu_R])^{-1}$  which arises from the geometrical sum of the *additional* Rayleigh waves around the half-cavity in the fundamental domain. These 1-cavity structures, which lead to the leading resonances in the 1-cavity case, correspond here to poles in  $\text{Det } M_{A_1}$  which amplify the contributions of the Rayleigh orbits already at topological length one, but which also complicate the searches for nearby genuine multi-scattering resonances, the zeros of  $\text{Det } M_{A_1}$ . This is especially the case for the family *i-add*.

Below  $\text{Re } k_L a \approx 32$ , SWA cycles of at most topological length two are needed to get a qualitative fit of the chaotic band labelled as *ii-lead*, whereas already order one is sufficient for the resonances *i-lead*, before they merge with the rising band *ii-ris* at about  $\text{Re } k_L a \approx 4$ , and for the resonances *i-add*. Below  $\text{Re } k_L a \approx 2$ , the SWA expansion breaks down and a uniform approximation based on a multipole expansion as in ref. [20] should take over. The dropping band, *iii-drop*, has a QM analog which is generated by Franz' creeping waves. The *regular* family of resonances (see *iii-reg* and *iv-reg*) corresponds to the  $t_L$  orbit that dominates the QM two-disk case [17], but is subdominant here, and that couples neither to the complex Rayleigh orbits nor to the shear orbit. When the *rising band* (*iv-ris*) crosses the regular band (*iii-reg*), the cumulant orders three and four are interchanged. It continues as band *iii-ris* and merges with the subleading band *ii-sub* at about  $\text{Re } k_L a = 35$ , generating the combined band *iii-sub*.

For the  $k_L$  window shown in fig. 1, the periodic orbit sum can be truncated at length four, since the spectrum generated from the cumulant expansion to this order does not differ from the complete one to the resolution of this figure. This is confirmed by numerical diagonalizations of the  $M \times M$  matrices  $M_{A_1}(k_L)$  in the  $\{\text{L}, \text{T}\} \times$  angular momentum space where  $M$  has to satisfy the bound  $M > e(c_L/c_T)|k_L|a$  (e.g.,  $M > 440$  for  $\text{Re } k_L = 45/a$ ) [8, 11].

*Summary and outlook.* – We have derived the scattering determinant and calculated, in the low-frequency regime, the exact scattering resonances and Wigner time delays for a quasi-two-dimensional isotropic and homogeneous elastodynamic slab with two cylindrical cavities. Already the physics of this simplest possible multi-scattering system in elastodynamics with free boundary conditions is totally different from the one of quantum billiards at low frequencies: none of the *measurable* medium excitation (*e.g.*, phase shifts, leading resonances) can be understood without the Rayleigh waves which do not have quantum-mechanical counterparts. For circular boundaries they are barely damped at all [7] and the diffraction constants, which link them at the different cavities to the shear waves, are still only weakly attenuated at low frequencies. These features are generic for smooth finite-size concave cavities. The pressure waves which are *the* analog of the scalar quantum-mechanical ones play only a secondary role.

A symbolic dynamics in the total space needs to account for cycles patched together from 4 kinds of segments: pressure, shear (their sum is the topological length), anti- and clockwise Rayleigh, implying an exponentially growing number of interfering periodic orbits. Whether the topological increase or the attenuation of the Rayleigh orbits eventually wins is still open. Surface orbits of Rayleigh type —with no counterpart in QM— are expected in general non-convex elastic resonators. Generalizations to anisotropic media (the highest- $Q$ -value experiments are performed on single crystals of quartz), and applications of the above ray-dynamics techniques to resonator geometries used in experiments remain open problems.

## REFERENCES

- [1] GUTZWILLER M. C., *Chaos in Classical and Quantum Mechanics* (Springer, New York) 1990.
- [2] CVITANOVIĆ P. *et al.*, *Chaos: Classical and Quantum* (ChaosBook.org, Copenhagen) 2005.
- [3] ELLEGAARD C., GUHR T., LINDEMANN K., NYGÅRD J. and OXBORROW M., *Phys. Rev. Lett.*, **77** (1996) 4918.
- [4] GRÄF H.-D. *et al.*, *Phys. Rev. Lett.*, **69** (1992) 1296.
- [5] ALT H. *et al.*, *Phys. Rev. Lett.*, **74** (1995) 62.
- [6] NEICU T. and KUDROLLI A., *Europhys. Lett.*, **57** (2002) 341.
- [7] IZBICKI J. L., CONOIR J. M. and VEKSLER N., *Wave Motion*, **28** (1998) 227.
- [8] BERRY M. V., *Ann. Phys. (N.Y.)*, **131** (1981) 163.
- [9] GASPARD P. and RICE S. A., *J. Chem. Phys.*, **90** (1989) 2225; 2242; 2255.
- [10] WIRZBA A., *Chaos*, **2** (1992) 77; *Nucl. Phys. A*, **560** (1993) 136.
- [11] WIRZBA A., *Phys. Rep.*, **309** (1999) 1; WIRZBA A., HENSELER M., *J. Phys. A*, **31** (1998) 2155.
- [12] LANDAU L. D. and LIFSHITZ E. M., *Theory of Elasticity* (Pergamon, Oxford) 1959.
- [13] COUCHMAN L., OTT E. and ANTONSEN T. M. jr., *Phys. Rev. A*, **46** (1992) 6193.
- [14] FRANZ W., *Z. Naturforschung*, **9a** (1954) 705.
- [15] SØNDERGAARD N., *Wave Chaos in Elastodynamic Scattering*, PhD Thesis (Northwestern University, Evanston) (2000); [www.nbi.dk/~nsonderg](http://www.nbi.dk/~nsonderg).
- [16] KELLER J. B. and KARAL F. C. jr., *J. Acoust. Soc. Am.*, **36** (1964) 32.
- [17] VATTAY G., WIRZBA A. and ROSENQVIST P. E., *Phys. Rev. Lett.*, **73** (1994) 2304.
- [18] ROSENQVIST P. E., VATTAY G. and WIRZBA A., *J. Stat. Phys.*, **83** (1996) 243.
- [19] SØNDERGAARD N. and TANNER G., *Phys. Rev. E*, **66** (2002) 066211.
- [20] ROSENQVIST P., WHELAN N. D. and WIRZBA A., *J. Phys. A*, **29** (1996) 5441.